

# Engineering the Electron Transport of Silicon-Based Molecular Electronic Devices via Molecular Dipoles

Nadine Gergel-Hackett,<sup>\*,†</sup> Izath Aguilar, and Curt A. Richter<sup>\*</sup>

Semiconductor Electronics Division, MS 8120, National Institute of Standards and Technology, 100 Bureau Dr., Gaithersburg, Maryland 20899

Received: June 29, 2010; Revised Manuscript Received: October 15, 2010

We demonstrate that charge transport through a CMOS-compatible molecular electronic device is dominated by one of two different transport regimes depending on the dipole of the molecular monolayer in the junction, doping level of the silicon substrate, and bias applied to the device. The two observed transport regimes are (1) a regime where the transport is limited by the Schottky barrier and the molecular dipole results in silicon band-bending at the junction interface and (2) a tunneling regime where the molecular dipole creates a small local electric field that screens the electrical transport.

## I. Introduction

The realization of molecular electronics will require the development of a practical molecular device with the potential for integration with existing technologies, as well as an improved understanding of the electron transport through Si/molecular monolayer/metal junctions.<sup>1</sup> We demonstrate the ability to engineer the electrical behavior of an enclosed silicon/molecular monolayer/metal device in a predictable manner, which contributes not only to the development of a CMOS-compatible molecular electronic technology but also to the understanding of electron transport in silicon-based structures. This work suggests a transport model for the silicon/molecular monolayer/metal system where no single variable acts in isolation; rather, it highlights how sensitive the system is to the dipole of the molecule used, as well as secondary effects including the doping of the silicon substrate and the applied bias.

Although great strides have been made toward fabricating silicon-based molecular devices and understanding the physics behind the charge transport through the junctions,<sup>2–15</sup> the complete picture is not yet fully developed. For example, many of the studies in the field of molecular electronics are performed by using a soft top electrical contact (such as mercury drops, carbon nanotubes, or electrolytes)<sup>15–19</sup> or an impermanent top contact (such as a conducting probe tip or wire)<sup>20,21</sup> in order to avoid the degradation of the molecular monolayer that can occur during the evaporation of a hard top contact.<sup>22,23</sup> Yet, because the electrical characteristics of the junction are dependent on the transport through the entire system, including effects from the contacts, it is difficult to extrapolate the implications of the studies performed with nonintegratable methodologies to real-world devices.<sup>1</sup> Our use of an enclosed device that is fabricated by using CMOS-compatible materials, as well as our statistical approach achieved by fabricating and characterizing hundreds of devices over multiple experimental runs, demonstrate the potential for the integration of the devices with traditional technologies and the extrapolation of the results from our study to real-world devices.<sup>2,24</sup>

Our work also builds on and enhances the existing work in the field in a significant way through the careful consideration of all parameters that can affect electrical transport (e.g., molecular backbone, molecular attaching group, and the doping level of the Si substrate). Motivated by the complexity of electron transport through a conjugated molecular/Si system,<sup>3–6,15</sup> we use unconjugated alkyl molecules that exhibit simple quantum mechanical tunneling in order to isolate the individual factors, such as molecular dipole and silicon doping, that affect the transport.<sup>7–14</sup> Additionally, whereas previous work explored the effect of molecular dipoles on the device's electrical characteristics by using molecules with different attachment chemistry assembled on n-type Si,<sup>14</sup> we vary the dipoles by changing the body of the molecules without changing the attachment chemistry. Because the attachment chemistry affects not only the dipole of the molecule but also the charge transfer between the molecule and Si,<sup>26</sup> by not altering the attachment chemistry, we can ensure that any differences observed between samples can be directly attributed to differences in the molecular dipole. To explore how changing the energetics of the Si affects charge transport, we tested molecular devices fabricated with both n-type and p-type Si substrates of different doping levels. The final result is a large systematic study of the effects of dipoles and substrate doping on the energetics of molecular devices with CMOS-integration potential both to better understand molecular-scale transport and to enable the engineering of devices with the desired electrical properties.

## II. Experimental Methods

**1. Device Structures.** The basic device design is an enclosed planar structure consisting of a monolayer of organic molecules directly assembled on silicon, contacted with silver (Figure 1). Silver was chosen as the top contact material because of previous studies demonstrating that, unlike many metals, it does not completely displace the molecular monolayer in the junction.<sup>23</sup> The structures were fabricated by using traditional photolithography and oxidation similar to that used to fabricate traditional CMOS devices. The bottom silicon substrate (p-type (100)  $10^{19}$  cm<sup>-3</sup>, p-type (111)  $10^{17}$  cm<sup>-3</sup>, n-type (111)  $10^{19}$  cm<sup>-3</sup>, or n-type (100)  $>10^{20}$  cm<sup>-3</sup>) was first oxidized by using a standard dry thermal oxidation to form a thermal oxide 150–200 nm thick. Different orientations of silicon were used because of the

<sup>\*</sup> Corresponding authors. E-mail: nadinegh@mbc.edu (N.G.-H.); curtrichter@nist.gov (C.A.R.).

<sup>†</sup> Current address: Department of Chemistry and Physics, Mary Baldwin College, Staunton, VA 24401.

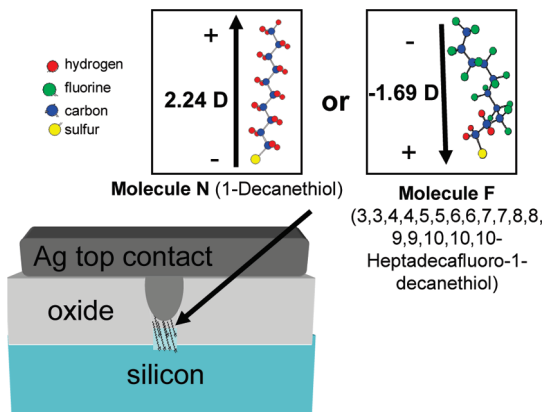


**Figure 1.** Device junction consisting of one of two different molecules assembled in a  $5 \mu\text{m} \times 5 \mu\text{m}$  well through an approximately  $150 \mu\text{m}$  thick silicon dioxide layer on a silicon substrate. Also shown is the relative free molecule dipole moment of each molecule.<sup>27</sup>

availability of substrates with the exact desired doping levels; however, previous work has demonstrated that wafer orientation does not affect the quality of monolayers assembled nor the electrical characteristics of the devices.<sup>2</sup>

Prior to molecular assembly, wells were etched in the thermal oxide of the silicon wafers. To form these wells, standard photolithography and a 6:1 buffered oxide were used to etch down through the thermal oxide and expose the surface of the underlying silicon wafer. Then, immediately prior to molecular assembly in the wells, the samples were etched with 2% HF for 30 s to remove any native oxide that may have formed and hydrogen-terminate the silicon in the bottom of the wells. The molecules were assembled directly on the bottom of the silicon well in a procedure described elsewhere by using UV-assisted assembly on the bottom well. The monolayers were prepared by utilizing UV reaction conditions following a procedure previously published.<sup>25</sup> Briefly, H-Si samples were immersed in a  $\text{CH}_2\text{Cl}_2$  solution containing  $\sim 10 \text{ mM}$  of 1-decanethiol or 3,3,4,4,5,5,6,6,7,7,8,8,9,9,10,10,10,10-heptadecafluoro-1-decanethiol and were illuminated for 2 h on each side by using a 6 W UV lamp (254 nm) with an intensity between  $30 \mu\text{W}/\text{cm}^2$  and  $1.5 \text{ mW}/\text{cm}^2$  at the sample in an inert environment. After illumination, the samples were rinsed with  $\text{CH}_2\text{Cl}_2$  and isopropyl alcohol. Care was used to ensure that the sample surface was immersed under solution during the entire time of radiation exposure while minimizing the total path length in solution.

After molecular assembly, the samples were removed from the solution, rinsed in dichloromethane, and immediately loaded for deposition of the top silver contact. The top contact was evaporated by using a slow ( $0.2 \text{ \AA}/\text{sec}$ ) thermal evaporation through a shadow mask over the wells. For control samples in our studies, we also fabricated molecule-free junctions from hydrogen-terminated Si, referred to as the controls (C). After the wells were etched, the exposed silicon surface at the bottom of the wells was hydrogen-terminated by immersing the silicon well in 2% HF for 30 s. The samples were then immediately loaded into the evaporator to be capped with Ag.

In order to study the effect of the molecular dipole on the electrical characteristics, we assembled one of two different types of monolayers with opposite free molecule dipole moments in each device. Figure 1 shows the radical dipole moments of each of the two molecules used in our devices.<sup>27</sup> The first molecule used is 1-decanethiol, a simple alkanethiol with a positive radical dipole moment of  $+2.24 \text{ D}$  that is referred to as the nonfluorinated molecule (N).<sup>27</sup> The second molecule is

3,3,4,4,5,5,6,6,7,7,8,8,9,9,10,10-heptadecafluoro-1-decanethiol. It has the same molecular backbone as the first but with 17 of the hydrogen atoms substituted by fluorine atoms, resulting in an opposite dipole (radical molecule value of  $-1.69 \text{ D}$ ) and is referred to as the fluorinated molecule (F). For control samples in our studies, we also fabricated molecule-free junctions from hydrogen-terminated Si, referred to as the controls (C).

**2. Electrical Characterization of Devices.** After fabrication, the devices were electrically characterized by using a commercial low-noise probe station. The top silver contact was directly probed, and a bias was applied between it and the substrate. All biases reported were to the top Ag contact, relative to the grounded silicon substrate. The resistance associated with the back-contact of the substrate was measured by comparing the resistance of two back-contacted devices individually with their combined resistance top-contacted in series. This back-contact resistance was found to be insignificant relative to the resistance of the molecular-device sizes and resistances that are reported in the work.

### III. Results and Discussion

It is theorized that the electrical transport through these devices occurs through two different regimes.<sup>7,28–31</sup> The first charge-transport regime is dominated by thermionic emission over the barrier that results from the band bending in the semiconductor near the molecular interface (the Schottky barrier).<sup>7,28–31</sup> This thermionic emission can be described by the general thermionic emission–diffusion model in eq 1,<sup>32</sup> where  $J$  is the current density,  $A$  is the Richardson constant,  $q$  is the electron charge,  $k$  is Boltzmann's constant,  $T$  is the temperature,  $n$  is the ideality factor,  $V$  is the applied bias, and  $q\phi_E$  is the effective Schottky barrier.<sup>32</sup> If there is a molecular monolayer forming a tunneling barrier in series with this Schottky barrier, tunneling may occur through the monolayer after thermionic emission over the Schottky barrier; however, the total electrical behavior is dominated by the effects of the Schottky barrier.

$$J = AT^2 e^{\left(\frac{-q\phi_E}{kT}\right)} e^{\left(\frac{qV}{nkT}\right)} (1 - e^{-qV/kT}) \quad (1)$$

In the second regime, there is an insignificant Schottky barrier, and transport is dominated by quantum mechanical tunneling through the potential-energy barrier formed by the molecular monolayer in the junction.<sup>7,28–31</sup> The existence of these two different transport regimes for alkyl monolayers on Si has been confirmed via variable-temperature measurements.<sup>31</sup> Additionally, it has been observed that the resistivity of the contacts (i.e., doping of the silicon substrate) can influence the transport through molecular junctions.<sup>7</sup> In order to study how the electrical transport is affected by the resistivity of the contacts, we varied not only the dipole of the molecular monolayer but also the doping of the silicon substrate. If the transport through the alkanethiols is a combination of thermionic emission and tunneling, depending on the dipole and silicon doping,<sup>7,28–31</sup> one would expect that, by systematically changing the type of the silicon (n or p-type), the doping level, and the dipole of the molecules used, one would observe systematic changes in trends in current. Thus, we fabricated devices with each of the two different dipole molecules on substrates of p-type silicon with a doping of  $10^{19} \text{ cm}^{-3}$ , p-type silicon with a doping of  $10^{17} \text{ cm}^{-3}$ , n-type silicon with a doping of  $10^{19} \text{ cm}^{-3}$ , and n-type silicon with a doping level of  $>10^{20} \text{ cm}^{-3}$ . We fabricated and electrically characterized 318 devices in total over seven

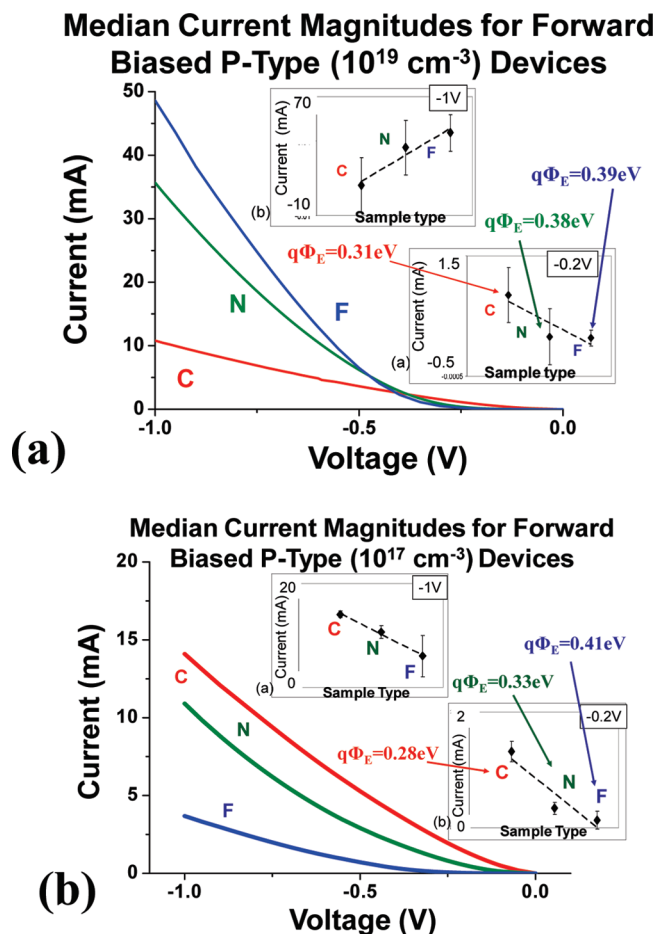


**Figure 2.** (a)  $I$ - $V$  curves representing the median electrical characterization of forward-biased devices assembled on p-type  $10^{19} \text{ cm}^{-3}$  Si with hydrogen-terminated silicon junctions (C), nonfluorinated molecules in the junctions (N), and fluorinated molecules in the junctions (F). (b)  $I$ - $V$  curves representing the median electrical characterization of forward-biased devices assembled on p-type  $10^{17} \text{ cm}^{-3}$  Si with hydrogen-terminated silicon junctions (C), nonfluorinated molecules in the junctions (N), and fluorinated molecules in the junctions (F). The insets show the median current values, including standard deviation, at relatively low bias ( $-0.2 \text{ V}$ ) and relatively high bias ( $-1.0 \text{ V}$ ). Also labeled on the insets are the  $q\Phi_E$  values for each molecular sample found by fitting eq 1 to the  $I$ - $V$  curve in the low bias regime.

different experimental runs. All devices that exhibited a current magnitude at  $0.2 \text{ V}$  of within  $\pm 1$  order of magnitude of the median value for each type of junction was included in the analysis (resulting in a yield of 287 out of 318 devices or approximately 90%).

**1. p-Type Silicon Molecular Devices.** Si/molecular monolayer/Ag samples were fabricated by self-assembling a molecular monolayer consisting of either nonfluorinated (N) molecules or fluorinated (F) molecules on p-type silicon with a doping level of approximately  $10^{19} \text{ cm}^{-3}$  and capping with Ag. Si/Ag control samples (C) were formed with hydrogen-terminated silicon. The median  $I$ - $V$  curves for each device biased in the forward direction (negative bias for p-type) are shown in Figure 2a. As these data show, there is a crossover point at approximately  $-0.4 \text{ V}$ , where the current magnitudes of the three different samples intersect. A crossover point similar to that in Figure 2a has been observed by several groups when studying the electrical characteristics ( $I$ - $V$  curves) of different alkyl molecules on semiconducting surfaces.<sup>7,28-32</sup> Such a curve has been theorized to be due to the electron transport being limited by the Schottky barrier between the top metal contact and the

bottom semiconducting substrate at relatively low bias and being limited by the quantum mechanical tunneling through the molecular monolayer at higher bias.<sup>7,28-31</sup>

The insets of Figure 2a show the median current values at  $-0.2$  and  $-1 \text{ V}$ , respectively, and demonstrate that, in the low bias regime ( $-0.2 \text{ V}$ ), the general trend is that the samples are most-to-least conducting in the order control (C), nonfluorinated (N), and fluorinated (F). The opposite trend is observed for the highly doped ( $10^{19} \text{ cm}^{-3}$ ) devices at relatively high bias ( $-1 \text{ V}$ ). In order to compare the low-bias trend in conductivity to theoretically predicted thermionic emission, we fit the current density for each curve in the low-bias regime to eq 1 to determine the effective Schottky barrier height ( $q\Phi_E$ ) and the ideality factor ( $n$ ). The effective Schottky barrier heights determined are labeled in the inset of Figure 2. These barrier heights are in the range of what is expected for the Schottky barrier of Ag-Si junctions ( $0.25$ – $0.69 \text{ eV}$ ).<sup>33</sup> The barrier heights are also consistent with our observed trend of sample conductivity in the low-bias regime: the more conductive a sample is at low bias, the smaller the barrier height found (because of the molecular shifting of the barrier as described below). The ideality factor for these samples ( $n$ ) ranges from 2.0 to 3.8, indicating that the transport through the barrier is not purely thermionic, as would be expected because of the presence of the molecular layer.

The current magnitude versus dipole trend at low bias is consistent with the expected effects of the molecular dipoles on the silicon bands at the interface.<sup>3</sup> Because Ag is a midgap metal, a positive molecular dipole results in upward bending of the silicon bands at the interface, and a negative molecular dipole moment results in downward bending of the silicon bands at the interface.<sup>3</sup> For p-type silicon, downward bending (negative dipole) results in an increased Schottky barrier and decreased current through a junction at low bias, when transport is Schottky-barrier limited (Figure 3a). Conversely, in this system, upward bending (positive dipole) results in a decreased Schottky barrier and increased current (Figure 3a). This explanation is consistent with the experimental observation that the molecule with the positive dipole (N) exhibits more current than the molecule with a negative dipole (F) for these p-type samples at low bias where the transport is limited by the Schottky barrier. The conduction of the hydrogen-terminated samples (C) is consistent with a junction that has an effective positive dipole at the interface even larger than that of the nonfluorinated samples N (2.24 D). Although one would expect hydrogen to introduce a small negative dipole when assembled on a silicon surface, because the control junctions lack an insulating layer between the silicon and metal (provided by the molecular layer in samples N and F), the expected effects of the H-Si dipole are not observed. Because the junction lacks a molecular tunnel junction, the shape and height of the barrier in the tunneling regime are also completely different than those of the molecular samples. The fact that the control sample does not exhibit characteristics consistent with a purely ohmic contact, as would be expected from a p+ Si-Ag junction,<sup>15</sup> is further evidence that these are not ideal Si-Ag junctions.

The detailed energetics of the junctions for the different molecules on p-type silicon at low bias (Schottky barrier limited regime) are illustrated via an energy-band diagram (Figure 3) and some basic equations (eqs 2-4). Figure 3 consists of the schematic energy-band diagrams for the different p-type silicon/molecular monolayer/metal junctions. The band bending at the silicon surface results from the energy offset between the Fermi level of the Ag and the electron affinity of the silicon and results

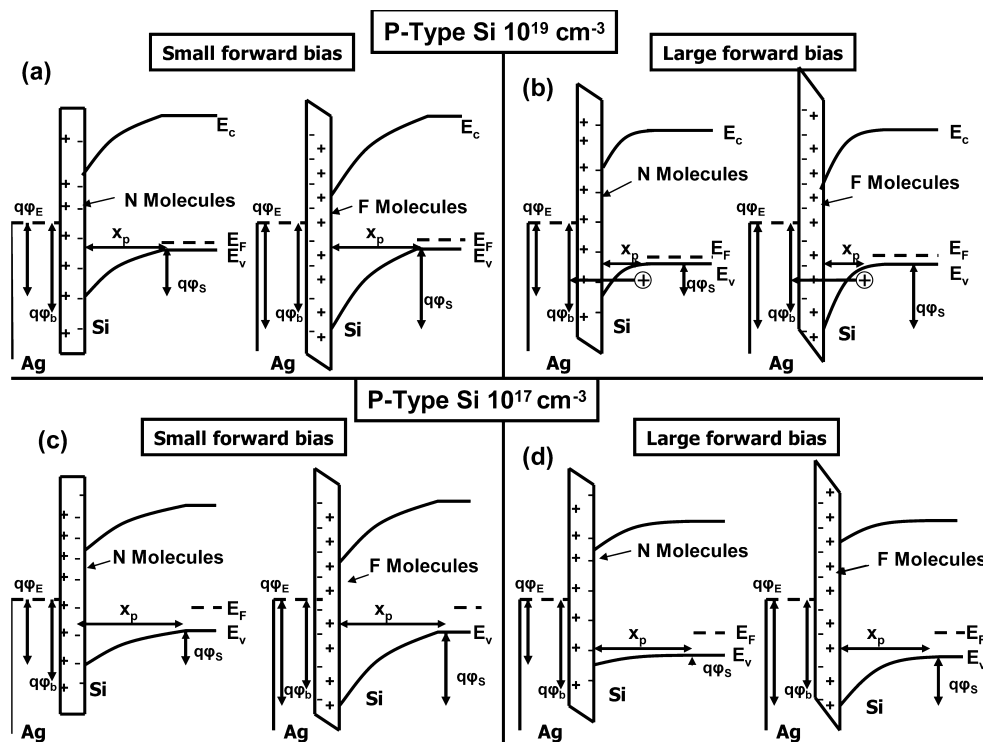


**Figure 3.** Schematic energy-band diagrams of the Ag/molecular monolayer/Si junctions with fluorinated (F) and nonfluorinated (N) monolayers assembled. (a) p-type Si  $10^{19} \text{ cm}^{-3}$  under relatively small forward bias, (b) p-type Si  $10^{19} \text{ cm}^{-3}$  under larger forward bias, (c) p-type Si  $10^{17} \text{ cm}^{-3}$  under relatively small forward bias, (d) p-type Si  $10^{17} \text{ cm}^{-3}$  under larger forward bias.

in what is known as the Schottky barrier ( $q\phi_b$ ). This Schottky barrier exists even though there is a molecular layer forming a tunneling barrier between the Ag top contact and Si surface, because the molecular barrier is thin enough that equilibrium charge transfer occurs between the Ag and Si, resulting in the band bending and the Schottky barrier. The molecular dipole changes the original Schottky barrier ( $q\phi_b$ ) by bending it up or down on the basis of the polarity of the dipole,<sup>3</sup> and the resulting barrier will be referred to as the effective Schottky barrier ( $q\phi_E$ , eq 2). The molecular dipole also creates an electric field at the Si–Ag interface that changes the shape of the molecular tunneling barrier.

$$q\phi_E = q\phi_b + \Delta$$

band bending due to molecular contribution (2)

$$q\phi_s = q\phi_E - (E_f - E_v) - qV$$

(for forward biased p-type silicon) (3)

$$q\phi_s = q\phi_E - (E_c - E_f) - qV$$

(for forward biased n-type silicon) (4)

The silicon surface barrier ( $q\phi_s$ ) represents the band bending within the silicon in the bulk near the interface with the molecular layer. For p-type silicon under forward bias, this band bending near the silicon ( $q\phi_s$ ) is equivalent to the effective Schottky barrier ( $q\phi_E$ ) minus the energy offset between the Fermi level of the silicon and the energy of the valence band ( $E_f - E_v$ ) minus the energy of the applied forward bias voltage ( $qV$ ), eq 3.<sup>33</sup> A similar relationship applies for forward-biased n-type silicon, but the energy offset is described by ( $E_c - E_f$ ), eq 4.<sup>33</sup> Because the energy offset between the Fermi level of the silicon and the valence/conduction band ( $E_f - E_v$  or  $E_c -$

$E_f$ ) is dependent on the magnitude of doping of the silicon,  $q\phi_s$  is also dependent on doping. The depletion region ( $X_p$ ) is the region near the interface where the silicon is depleted of majority carriers because of the equilibrium charge transfer between the Ag top contact and Si bottom contact. This depletion region ( $X_p$ ) is strongly inversely dependent on the level of silicon doping and also has a weak direct dependence on the magnitude of the silicon surface barrier  $q\phi_s$  (Figure 3).<sup>33</sup>

By referring to the energy-band diagram in Figure 3a, it is evident how, for the case of the  $I$ – $V$  curves in Figure 2a under low forward bias (0.2 V), the depletion width ( $X_p$ ) is relatively wide because of the moderate doping level and the relatively large surface band bending ( $q\phi_s$ ). Because, for this case, the depletion width is too wide to facilitate the quantum mechanical tunneling of holes through it, the transport will be dominated by thermionic emission over  $q\phi_s$ , or Schottky-barrier-dominated transport, as described by eq 1. As evident in eq 1, the current magnitude should be inversely proportional to the magnitude of  $q\phi_E$  (eq 1). Because the nonfluorinated molecules (N) decrease the effective Schottky barrier ( $q\phi_E$ ) of p-type silicon and the fluorinated molecules (F) increase the barrier (Figure 3),<sup>3</sup> the nonfluorinated molecular devices (N) should exhibit larger current than the fluorinated molecular devices (F). This expected trend in current versus dipole is consistent with both the trend in sample conductivity and the trend in fit effective Schottky barrier heights in Figure 2a, confirming that the electrical characteristics match the theoretical expectations. If the experimental results from the molecule-free hydrogen-terminated sample (C) are interpreted as arising from the dipole–molecular barrier system, they are still consistent with what one would expect from a junction with a positive effective dipole that is even larger than that of the nonfluorinated samples N (2.24 D).

Once the bias is increased sufficiently, the transport changes from the Schottky-barrier-limited regime to quantum mechanical tunneling through the molecular monolayer. As the bias of the

p-type Si is increased, approaching flatband conditions (Figure 3b), not only does  $q\phi_s$  decrease, but so does the width of the depletion region ( $X_p$ ). As this occurs,  $X_p$  approaches a barrier that is thin enough for holes to begin to tunnel through it and then through the additional tunneling barrier of the molecular monolayer (Figure 3b). The transport is then dominated by classic quantum mechanical tunneling, where the current is inversely proportional to the molecular tunneling barrier height, shape, and width.

When transport is occurring via quantum mechanical tunneling, the dipole of the molecular monolayer creates a small local electric field that screens or alters the effective tunneling barrier seen by the charge carriers tunneling through it. This field changes the potential drop over the molecular tunneling barrier, thus altering the height and shape of the molecular barrier and affecting the probability of electrons tunneling through it. For example, **N** molecules have a positive dipole relative to the surface of the silicon; thus, any holes approaching the molecular tunneling barrier from the silicon experience a negative electric field at the molecular tunneling barrier due to the positive molecular dipole. This negative electric field decreases the molecular tunneling barrier for the holes, increasing the tunneling current. However, the **F** monolayer exhibits a negative dipole relative to the silicon surface; therefore, the holes from the silicon would see a positive electric field, increasing the tunneling barrier for the holes and decreasing current. As the tunneling mechanism begins to dominate the transport, this effect of the dipole on the molecular tunneling barrier starts to dominate over the effect of the dipole on the Schottky barrier ( $q\phi_E$ ).

The reversal in the current magnitude trend of **N** and **F** samples before and after crossover (Figure 2a) is consistent with the expected opposite effects of the dipoles in each transport regime. At low bias, when the transport is dominated by the effects of the molecular dipole on the Schottky barrier (Figure 3a, eqs 1 and 2), the p-type samples with the more electronegative molecule (**F**) are less conductive; whereas at higher bias, the transport is dominated by the effects of the molecular dipole on the molecular tunneling barrier; therefore, the **F** sample is more conductive. It is important to note that, because the control device (**C**) does not have a molecular tunnel junction, the shape and height of the barrier in the tunneling regime are completely different than those of the molecular samples. Still, the experimental trends in the low- and high-bias regimes of the control sample (**C**), Figure 2, are consistent with what would be expected from a junction with a more positive surface dipole (relative to the silicon surface) than the devices with the **N** molecules.

We also fabricated devices containing the same types of monolayers (**C**, **N**, and **F**), but on p-type silicon with a lower  $10^{17}$  doping. The  $I$ - $V$  curves for these devices are shown in Figure 2b, and these curves show a trend similar to that observed from the p-highly doped (Figure 2a) at low bias (0.2 V); however, no crossover is observed as the devices are biased up to  $-1$  V. These data are indicative that these devices with relatively lightly doped silicon do not leave the Schottky-barrier-dominated transport regime (eq 1) even under increased bias. As illustrated in Figure 3c,d, the depletion region that results from the Schottky barrier for these devices is still too wide for the device to enter the tunneling regime, even when up to  $-1$  V is applied; hence, no crossover is observed in the electrical characteristics. It is expected that a crossover would be observed at a higher applied bias; however, we did not characterize the devices with bias magnitudes greater than 1 V because of

concerns with catastrophic device failure at higher bias. These  $I$ - $V$  curves at all biases in Figure 2b are consistent with the trend expected for the Schottky-barrier-limited transport regime (the current for sample **C** is greater than that for **N**, which is greater than that for **F**), which is the same trend as that in Figure 2a at low bias.

**2. n-Type Silicon Molecular Devices.** Similar devices were fabricated from  $10^{19}$  doped n-type silicon. For these devices, one would expect the opposite trends in current in the low-bias (0.2 V) regime than those that were observed for the  $10^{19}$  p-type silicon. This flip in trends is expected because transport in p-type silicon occurs through the valence band ( $E_v$ ); therefore, a downward bending in the bands that results from a negative surface dipole (**F**) increases the Schottky barrier (relative to the dipole-neutral band position and barrier); whereas for n-type Si, the transport occurs through the conduction band ( $E_c$ ); therefore, a downward band bending decreases the effective Schottky barrier ( $q\phi_E$ ) from its dipole-neutral position (eq 1, Figure 4). The resulting decreased Schottky barrier should increase the current for the low-bias regime where the transport is Schottky-barrier limited (i.e.,  $\Delta$  band bending due to molecular contribution in eq 1 is negative).

The expected trend in median current for devices on  $10^{19}$   $\text{cm}^{-3}$  n-type silicon at low bias (0.2 V) is observed (Figure 5a). The median current of sample **F** is greater than that of **N**, which is greater than the median current of **C**. This trend is opposite of that observed from the  $10^{19}$  p-type silicon at low bias (Figure 2a). This trend is consistent with the proposed method of transport at low bias being dominated by the molecular effects on the Schottky barrier due to a wide  $X_p$  (Figure 4a), which would affect the magnitude of the electrical transport oppositely for n-type junctions as it would for p-type. The effective Schottky barrier heights (labeled in the inset) are consistent with our observed trend of sample conductivity in the low-bias regime. The ideality factor for these samples ( $n$ ) ranges from 1.1 to 1.2 for the moderately doped samples and from 4.0 to 4.1 for the degenerately doped samples. These values suggest that the transport through the moderately doped n-type samples is the closest to purely thermionic emission, which is consistent with the fact that the moderately doped n-type samples exhibit approximately three orders of magnitude less current in the low-bias regime than the other samples.

This observed switch in trend between the n-type and p-type devices serves as additional confirmation that the experimental results are consistent with the model.

At relatively high bias, a crossover between the median current magnitudes of **N** and **F** samples occurs, where **N** samples start to exhibit greater conductivity than **F** samples (Figure 5a). This high-bias regime trend of **N** samples exhibiting greater conductivity than **F** samples on n-type  $10^{19}$  Si (Figure 5a) is opposite to what was observed for the p-type  $10^{19}$  devices where **F** samples were more conductive than **N** samples (Figure 2a). This reversal in trend is as expected and is consistent with the trend in effective Schottky barrier heights observed via fitting the low-bias  $I$ - $V$  curves to eq 1. In the relatively high-bias regime, the applied bias is large enough to result in a negligible  $X_p$  (Figure 4b). In this regime, the molecular effects dominate through the screening of the tunneling electrons or holes (electrons in the case of n-type Si) by the electric field that results from the dipole of the molecular monolayer. Because electrons are the majority carrier (and hence tunneling particle) of n-type silicon, the screening effect of the molecular dipole will be opposite of that for positively charged holes (p-type silicon).

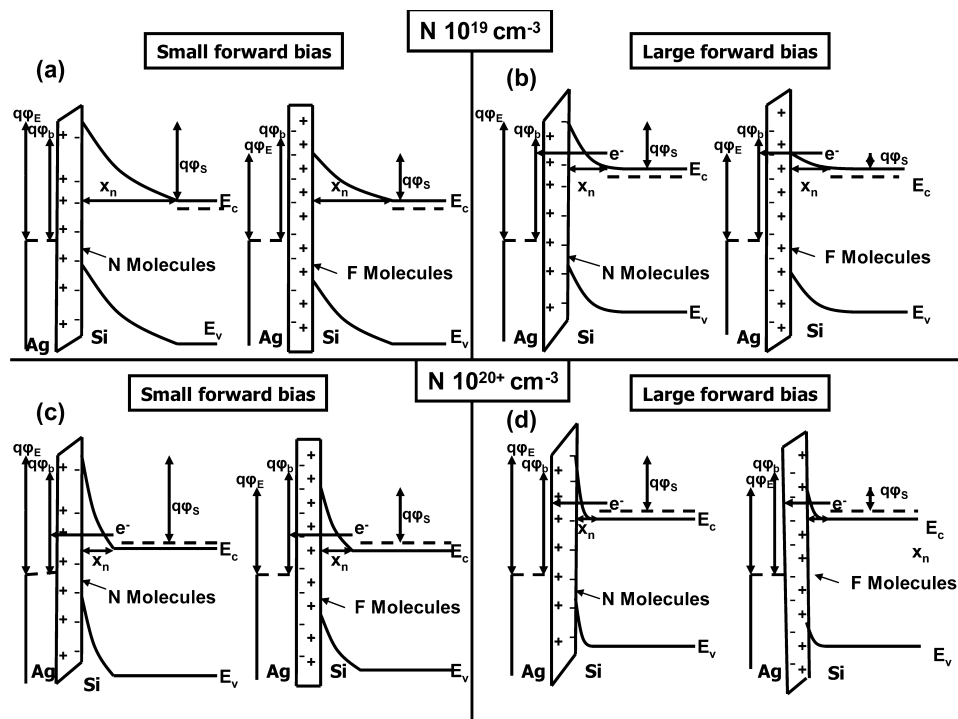


**Figure 4.** Schematic energy-band diagrams of the Ag/molecular monolayer/Si junctions with fluorinated (F) and nonfluorinated (N) monolayers assembled. (a) n-type Si  $10^{19} \text{ cm}^{-3}$  under relatively small forward bias, (b) n-type Si  $10^{19} \text{ cm}^{-3}$  under larger forward bias, (c) n-type Si  $> 10^{20} \text{ cm}^{-3}$  under relatively small forward bias, (d) n-type Si  $> 10^{20} \text{ cm}^{-3}$  under larger forward bias.

As shown in the inset of Figure 5a, the conductivity of the control sample (C) at 1 V is still lower than that of either the F or the N sample at 1 V (crossover did not yet occur for sample type C). The lack of a crossover for the control sample (C) indicates that  $10^{19} \text{ cm}^{-3}$  doping for n-type silicon is not adequate for the control sample (which has a larger  $X_p$  relative to samples N or F because of its strongly positive molecular dipole) to have transitioned from Schottky-barrier-limited transport to tunneling. This transition in transport regimes occurs by a magnitude of 1 V for the C sample on p-type silicon but not for the C sample on n-type silicon, because the dipole of the monolayer that increases the Schottky barrier the most for p-type Si, monolayer F, is 1.69 D, whereas the effective dipole that increases the Schottky barrier the most for the n-type Si, the dipole of sample C, is greater than that of molecule N of 2.24 D (based on its electrical results relative to the known dipole of monolayer N). Because the magnitude of the dipole of the limiting sample (C) on n-type is considerably larger than that of the limiting sample (F) on p-type, all three samples (F, N, and C) transition to tunneling by 1 V on p-type silicon, but C on n-type does not transition by 1 V. In order to observe this transition for all three samples on n-type silicon at 1 V, more highly doped silicon is required.

In order to observe this transition by decreasing the depletion width  $X_p$  (Figure 4c,d) and thereby increasing the probability of tunneling, we fabricated and characterized devices by using degenerately n-type doped Si ( $> 10^{20} \text{ cm}^{-3}$ ). The electrical results from these samples (Figure 5b) and the current magnitude trends in both the high- and low-bias regimes are consistent with the expected trend of the lower doped ( $10^{19} \text{ cm}^{-3}$ ) n-type silicon (Figure 5a) in the tunneling (higher bias) regime. These data indicate that, for these n-type degenerately doped Si samples,  $X_p$  is adequately thin for the electrons to tunnel from the Si to the Ag at all biases (Figure 4c,d), and thus, the tunneling mechanism and its associated trends dominate at all biases. Overall, the trend observed from the electrical results and

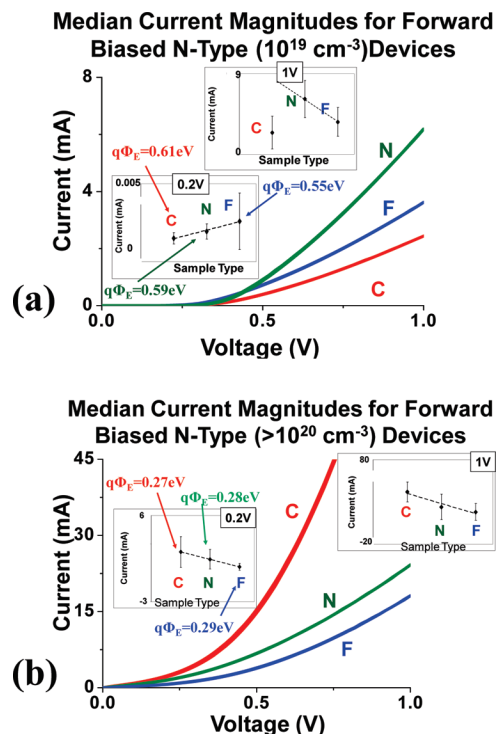


**Figure 5.** (a)  $I$ - $V$  curves representing the median electrical characterization of forward-biased devices assembled on n-type  $10^{19} \text{ cm}^{-3}$  Si with hydrogen-terminated silicon junctions (C), nonfluorinated molecules in the junctions (N), and fluorinated molecules in the junctions (F). (b)  $I$ - $V$  curves representing the median electrical characterization of forward-biased device assembled on n-type  $> 10^{20} \text{ cm}^{-3}$  Si with hydrogen-terminated silicon junctions (C), nonfluorinated molecules in the junctions (N), and fluorinated molecules in the junctions (F). The insets show the median current values, including standard deviation, at relatively low bias (0.2 V) and relatively high bias (1.0 V). Also labeled on the insets are the  $q\Phi_E$  values for each molecular sample found by fitting eq 1 to the  $I$ - $V$  curve in the low-bias regime.

effective Schottky barrier height fits from **N**, **F**, and **C** on the degenerately doped n-type silicon is consistent with the transport methods proposed.

#### IV. Conclusions

We performed a large systematic study of the effect of molecular dipole on the electrical behavior of enclosed, planar, silicon-based, molecular electronic devices, and we were able to control the electrical behavior of the devices by varying the molecular dipole and silicon doping. Experimental results and the fit of these results to the general thermionic emission–diffusion model for the Schottky-barrier-limited regimes (generally relatively low bias) were consistent with a positive molecular dipole resulting in upward bending of the silicon bands at the interface and a negative molecular dipole moment resulting in downward bending of the silicon bands at the interface. Experimental results in the regimes dominated by tunneling through the molecular barrier (relatively high bias) were consistent with the dipole of the molecular monolayer creating a small local electric field that screens the effective tunneling barrier seen by the electrons/holes tunneling through it. By establishing the dipole-dependent electrical behavior of the devices, we not only gained an understanding of the energetics of the device but also also demonstrated the potential for future engineering of molecular electronic devices that are compatible with the existing state-of-the-art CMOS technology.

**Acknowledgment.** We thank Jim Kushmerick and Mariona Coll Bau for helpful conversations and Christina Hacker for help with molecular figures. This work was funded in part by the NIST Office of Microelectronics Programs. The research was performed while N.G.H. held a National Research Council Research Associate Award and I.N.A. was a NSF Summer Undergraduate Research Fellow at the National Institute of Standards and Technology.

#### References and Notes

- (1) Ratner, M. Molecular Electronics: Charged with Manipulation. *Nature* **2005**, *435*, 575–577.
- (2) Gergel-Hackett, N.; Zangmeister, C. D.; Hacker, C. A.; Richter, L. J.; Richter, C. A. Demonstration of Molecular Assembly on Si (100) for CMOS-Compatible Molecule-Based Electronic Devices. *J. Am. Chem. Soc.* **2008**, *130* (13), 4259–4261.
- (3) Hiremath, R. K.; Rabinal, M. K.; Mulimani, B. G.; Khazi, I. M. Molecularly Controlled Metal-Semiconductor Junctions on Silicon Surface: A Dipole Effect. *Langmuir* **2008**, *24*, 11300–11306.
- (4) Hunger, R.; Jaegermann, W.; Merson, A.; Shapira, Y.; Pattenkofer, C.; Rappich, J. Electronic Structure of Methoxy-, Bromo-, and Nitrobenzene Grafted onto Si(111). *J. Phys. Chem. B* **2006**, *110*, 15432–15441.
- (5) Scott, A.; Janes, D. B.; Risko, C.; Ratner, M. A. Fabrication and Characterization of Metal-Molecule-Silicon Devices. *Appl. Phys. Lett.* **2007**, *91*, 033508–1:033508–3.
- (6) He, T.; Corley, D. A.; Lu, M.; Halen Di Spigna, N.; He, J.; Nackashi, D. P.; Franzon, P. D.; Tour, J. M. Controllable Molecular Modulation of Conductivity in Silicon-Based Devices. *J. Am. Chem. Soc.* **2009**, *131* (29), 10023–10030.
- (7) Saloman, A.; Boecking, O.; Seitz, O.; Markus, T.; Amy, F.; Chan, C.; Zhao, W.; Cahen, D.; Kahn, A. What is the Barrier for Tunneling Through Alkyl Monolayers? Results from n- and p-Si-Alkyl/Hg Junctions. *Adv. Mater.* **2007**, *19*, 445–450.
- (8) Cui, X. D.; Zarate, X.; Tomfohr, J.; Sankey, O. F.; Primak, A.; Moore, A. L.; Moore, T. A.; Gust, D.; Harris, G.; Lindsay, S. M. Making Electrical Contacts to Molecular Monolayers. *Nanotechnology* **2002**, *13*, 5–14.
- (9) Wold, D. J.; Frisbie, C. D. Fabrication and Characterization of Metal-Molecule-Metal Junctions by Conducting Probe Atomic Force Microscopy. *J. Am. Chem. Soc.* **2001**, *123*, 5549–5556.
- (10) Wang, W.; Lee, T.; Reed, M. A. Mechanism of Electron Conduction in Self-Assembled Alkanethiol Monolayer Devices. *Phys. Rev. B* **2003**, *68*, 035416.
- (11) Majumdar, N.; Gergel, N.; Routenberg, J. M.; Bean, J. C.; Harriott, L. R.; Li, B.; Pu, L.; Yao, Y.; Tour, J. M. Nanowell Device for the Electrical

Characterization Of Metal-Molecule-Metal Junctions. *J. Vac. Sci. Technol., B: Microelectron. Nanometer Struct.—Process., Meas., Phenom.* **2005**, *23* (4), 1417–1421.

- (12) Wang, W.; Scott, A.; Gergel-Hackett, N.; Hacker, C. A.; Janes, D. B.; Richter, C. A. Probing Molecules in Integrated Silicon-Molecule-Metal Junctions by Inelastic Tunneling Spectroscopy. *Nano Lett.* **2008**, *8* (2), 478–484.

- (13) Yu, L. H.; Gergel-Hackett, N.; Zangmeister, C. D.; Hacker, C. A.; Richter, C. A.; Kushmerick, J. G. Molecule-Induced Interface States Dominate Charge Transport in Si-Alkyl-Metal Junctions. *J. Phys.: Condens. Matter* **2008**, *20*, 374114–374119.

- (14) Thieblemont, F.; Seitz, O.; Vilan, A.; Cohen, H.; Salomon, E.; Kahn, A.; Cahen, D. Electronic Current Transport through Molecular Monolayers: Comparison between Hg/Alkoxy and Alkyl Monolayer/Si(100) Junctions. *Adv. Mater.* **2008**, *20*, 3931–3936.

- (15) Hiremath, R. K.; Rabinal, M. H. K.; Mulimani, B. G. Dipole Tuning of Charge Transport in Molecular Junctions. *Phys. Chem. Chem. Phys.* **2010**, *12*, 2564–2586.

- (16) Roth, K. M.; Yasseri, A. A.; Liu, Z.; Dabke, R. B.; Malinovsky, V.; Schweikart, K. H.; Yu, L.; Tiznado, H.; Zaera, F.; Lindsey, J. S.; Kuhr, W. G.; Bocian, D. F. Measurements of Electron-Transfer Rates of Charge-Storage Molecular Monolayers on Si(100). Toward Hybrid Molecular/Semiconductor Information Storage Devices. *J. Am. Chem. Soc.* **2003**, *125*, 505–517.

- (17) Faber, E. L.; De Smet, L. C. P. M.; Olthius, W.; Zuilhof, H.; Sudholter, E. J. R.; Bergveld, P.; Van de Berg, A. Si-C Linked Organic Monolayers on Crystalline Silicon Surfaces as Alternative Gate Insulators. *ChemPhysChem* **2005**, *6*, 2153–2166.

- (18) He, J.; Chen, B.; Flatt, A. K.; Stephenson, L. J.; Coyle, C. D.; Tour, J. M. Metal-Free Silicon-Molecule-Nanotube Testbed and Memory Device. *Nat. Mater.* **2006**, *5*, 63–68.

- (19) Coll, M.; Miller, L. H.; Richter, L. J.; Hines, D. R.; Jurchescu, O. D.; Gergel-Hackett, N.; Richter, C. A.; Hacker, C. A. Formation of Silicon-Based Molecular Electronic Structures Using Flip-Chip Lamination. *J. Am. Chem. Soc.* **2009**, *131* (34), 12451–12457.

- (20) Wold, D. J.; Frisbie, C. D. Fabrication and Characterization of Metal-Molecule-Metal Junctions by Conducting Probe Atomic Force Microscopy. *J. Am. Chem. Soc.* **2001**, *123*, 5549–5556.

- (21) Kushmerick, J. G.; Holt, D. B.; Yang, J. C.; Naciri, J.; Moore, M. H.; Shashidhar, R. Metal-Molecule Contacts and Charge Transport across Monomolecular Layers: Measurement and Theory. *Phys. Rev. Lett.* **2002**, *89*, 086802.

- (22) Walker, A. V.; Tighe, T. B.; Cabarcos, O. M.; Reinard, M. D.; Haynie, B. C.; Uppili, S.; Winograd, N.; Allara, D. L. The Dynamics of Noble Metal Atom Penetration through Methoxy-Terminated Alkanethiolate Monolayers. *J. Am. Chem. Soc.* **2004**, *126*, 3954–3963.

- (23) Hacker, C. A.; Richter, C. A.; Gergel-Hackett, N.; Richter, L. J. Origin of Differing Reactivities of Aliphatic Chains on H-Si(111) and Oxide Surfaces with Metal. *J. Phys. Chem. C* **2007**, *111* (26), 9384–9392.

- (24) Rose, G. S.; Yao, Y. X.; Tour, J. M.; Cabe, A. C.; Gergel-Hackett, N.; Majumdar, N.; Bean, J. C.; Harriott, L. R.; Stan, M. R. Designing CMOS/Molecular Memories While Considering Device Parameter Variations. *ACM J. Emerg. Technol.* **2007**, *3* (1), 1–24.

- (25) Hacker, C. A.; Anderson, K. A.; Richter, L. J.; Richter, C. A. *Langmuir* **2005**, *21*, 882–889.

- (26) Hacker, C. A. Modifying Electron Transfer at the Silicon-Molecule Interface using Atomic Tethers. *Solid State Elec.* Submitted.

- (27) Campbell, I. H.; Rubin, S.; Zawodzinski, T. A.; Kress, J. D.; Martin, R. L.; Smith, D. L.; Baarashkov, N. N.; Ferraris, J. P. Controlling Schottky Energy Barriers in Organic Electronic Devices using Self-Assembled Monolayers. *Phys. Rev. B* **1996**, *54* (20), 14321–14324.

- (28) Saloman, A.; Boecking, T.; Chan, C. K.; Amy, F.; Girchevitz, O.; Cahen, D.; Kahn, A. How Do Electronic Carriers Cross Si-Bound Alkyl Monolayers. *Phys. Rev. Lett.* **2005**, *95*, 266807:1–266807:4.

- (29) Seitz, O.; Bocking, T.; Saloman, A.; Gooding, J. J.; Cahen, D. Importance of Monolayer Quality for Interpreting Current Transport through Organic Molecules: Alkyls on Oxide-Free Si. *Langmuir* **2006**, *22*, 6915–6922.

- (30) Bocking, T.; Saloman, A.; Cahen, D.; Gooding, J. J. Thiol-Terminated Monolayers on Oxide-Free Si: Assembly of Semiconductor-Alkyl-S-Metal Junctions. *Langmuir* **2007**, *23*, 3236–3241.

- (31) Saloman, A.; Shpaisman, H.; Seitz, O.; Boecking, T.; Cahen, D. J. Temperature-Dependent Electronic Transport through Alkyl Chain Monolayers: Evidence for a Molecular Signature. *Phys. Chem. C* **2008**, *112*, 3969–3974.

- (32) Faber, E. J.; de Smet, L. C. P. M.; Olthius, W.; Zuilhof, H.; Sudholter, E. J. R.; Bergveld, P.; van de Berg, A. Si-C Linked Organic Monolayers on Crystalline Silicon Surfaces as Alternative Gate Insulators. *ChemPhysChem* **2005**, *6*, 2153–2166.

- (33) Neamen, D. A. *Semiconductor Physics and Devices*, Vol. 2; Isenberg, S., Butcher, K., Eds.; Irwin/McGraw-Hill: USA, 1997; p 312.